CORA Cork Open Research Archive
Cartlann Taighde Oscailte Chorcaí

Title	A frequency transformation for co-designed multi-passband/ multi-embedded-notch RF filters
Authors	Gómez-García, Roberto;Yang, Li;Psychogiou, Dimitra
Publication date	2021-02-02
Original Citation	Gómez-García, R., Yang, L. and Psychogiou, D. (2021) 'A frequency transformation for co-designed multi-passband/ multi-embedded-notch RF filters', IEEE Transactions on Circuits and Systems II: Express Briefs, 68(7), pp.2429-2433. https://doi.org/10.1109/TCSII.2021.3056584
Type of publication	Article (peer-reviewed)
Link to publisher's version	10.1109/TCSII.2021.3056584
Rights	© 2021, IEEE. Personal use of this material is permitted. Permission from IEEE must be obtained for all other uses, in any current or future media, including reprinting/republishing this material for advertising or promotional purposes, creating new collective works, for resale or redistribution to servers or lists, or reuse of any copyrighted component of this work in other works.
Download date	2026-11-06 17:27:45
Item downloaded from	https://hdl.handle.net/10468/11137



University College Cork, Ireland
Coláiste na hOllscoile Corcaigh

This article has been accepted for publication in a future issue of this journal, but has not been fully edited. Content may change prior to final publication. Citation information: DOI 10.1109/TCSII.2021.3056584, IEEE Transactions on Circuits and Systems II: Express Briefs

A Frequency Transformation for Co-Designed Multi-Passband/Multi-Embedded-Notch RF Filters

Roberto Gómez-García, *Senior Member, IEEE*, Li Yang, *Member, IEEE*, and Dimitra Psychogiou, *Senior Member, IEEE*

***Abstract*—A class of multi-resonant RF filtering stage that exhibits a multi-band bandpass filtering transfer function with embedded in-band notches is presented. It is derived from the application of a composed lowpass-to-multi-passband/multi-stopband frequency transformation that converts the normalized lowpass prototype into the proposed multi-passband/multi-embedded-notch filtering cell. Thus, when employed in higher-order filtering networks, high-selectivity multi-band bandpass-filter (BPF) counterparts with embedded in-band stopbands are synthesized. Furthermore, two different approaches for out-of-band transmission-zero (TZ) generation in these type of filters to achieve sharp-rejection characteristics into them are detailed. The operational foundations of the engineered multi-passband/multi-embedded-notch filtering stage are described, along with several illustrative first-to-multi-order theoretical design examples with/without stopband TZs. Moreover, for experimental-demonstration purposes, a proof-of-concept microstrip prototype of a third-order dual-band BPF with two and one embedded notches in its lower and upper transmission bands, respectively, is manufactured and characterized.**

***Index Terms*—Bandpass filter (BPF), bandstop filter (BSF), microstrip filter, microwave filter, multi-band filter, multi-functional filter, notch filter, planar filter, RF filter, transmission zero (TZ).**

I. Introduction

Modern multi-standard high-frequency transceivers must process multiple RF signals in the same module while accessing a highly-congested radio spectrum. As such, the need for advanced pre-selection microwave filters with various passbands (multi-RF-signal acquisition) and multi-notched-band capability (multi-interference suppression) is highly desired in emerging RF multi-standard interference-dominant telecommunication scenarios, including multi-band multi-carrier communication systems. However, prior-art multi-band filters have focused on multi-passband (e.g., [1]–[7] for single-ended and differential-mode/balanced topologies) or multi-stopband (e.g., [8]–[10]) applications separately, with almost no examples joining both functionalities—apart from their direct in-series cascade which increases circuit size and insertion loss. On the other hand, the integration of in-band notches—frequency-static, switchable, or spectrally-agile ones either with reflective-type or absorptive/reflectionless nature—in bandpass filters (BPFs) has been mostly restricted to single-band designs [11]–[15].

Manuscript received November 8, 2020; revised January 10, 2021; accepted January 31, 2021. This work was supported in part by the Spanish Ministry of Economy, Industry, and Competitiveness (State Research Agency) under Project TEC2017-82398-R, in part by the GOT ENERGY TALENT (GET) fellowship programme co-funded by the EU as part of the H2020-MSCA-COFUND programme (Grant Agreement number 754382), and in part by the National Science Foundation under Grant ECCS-1731956. *(Corresponding author: Roberto Gómez-García.)*

R. Gómez-García and L. Yang are with the Department of Signal Theory and Communications, University of Alcalá, Alcalá de Henares 28871, Madrid, Spain (e-mails: roberto.gomez.garcia@ieee.org; li.yang@uah.es).

D. Psychogiou was with the Department of Electrical, Computer, and Energy Engineering, University of Colorado Boulder, Boulder, CO 80309, USA. She is now with the Department of Electrical and Electronic Engineering, University College Cork, and Tyndall National Institute, Cork, Ireland (e-mail: dpsychogiou@ucc.ie).

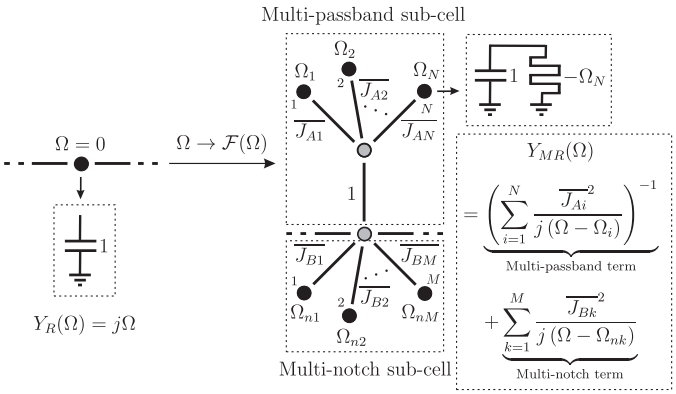


Fig. 1. Normalized coupling-routing diagram of the proposed N-passband/M-embedded-notch filtering stage after applying the frequency transformation $\Omega \to \mathcal{F}(\Omega)$ in (1) over a normalized lowpass resonating node (black circles: resonating nodes; grey circles: zero-susceptance non-resonating nodes; continuous lines: couplings; $Y_R(\Omega)$ and $Y_{MR}(\Omega)$: input admittances of the lowpass resonator and the multi-resonant cell, respectively).

A multi-resonant RF filtering stage with co-designed multi-passband/multi-embedded-notch response is reported. This double-behavior filtering cell is applied to the realization of high-order filtering networks with/without stopband transmission zeros (TZs), which can exhibit an arbitrary number of passbands and in-band notches. When compared to the in-series cascade connection of a multi-passband and various in-band-notch filtering units to realize the same composite filtering transfer function, smaller circuit size is achieved through this filter design methodology as several admittance inverters are shared/reused by both filtering functionalities. The theoretical foundations of this co-designed RF filter approach by using frequency-transformation and coupling-routing-diagram techniques—analytical framework that is general for any analog-circuit technology and frequency band [16]—are detailed in Section II. In Section III, a dual-passband/triple-in-band-notch filter prototype is built in microstrip technology and tested for experimental-validation purposes.

II. Theoretical Foundations

This section presents the theoretical operational principles of the proposed co-designed multi-passband/multi-embedded-notch RF filtering stage. Afterwards, in-series-cascade designs for higher-order filter realizations and two different strategies

1549-7747 (c) 2021 IEEE. Personal use is permitted, but republication/redistribution requires IEEE permission. See http://www.ieee.org/publications_standards/publications/rights/index.html for more information.
Authorized licensed use limited to: UNIVERSITY COLLEGE CORK. Downloaded on March 10,2021 at 10:54:12 UTC from IEEE Xplore. Restrictions apply.

This article has been accepted for publication in a future issue of this journal, but has not been fully edited. Content may change prior to final publication. Citation information: DOI 10.1109/TCSII.2021.3056584, IEEE Transactions on Circuits and Systems II: Express Briefs

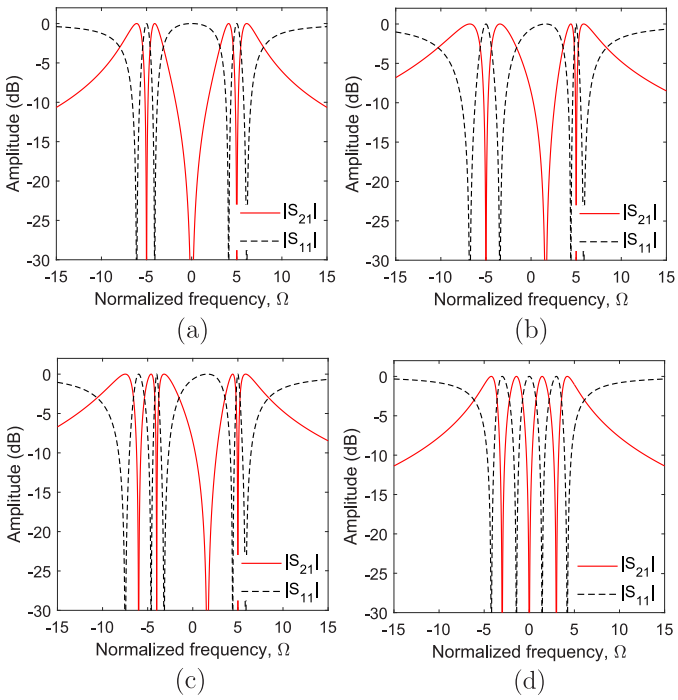


Fig. 2. Examples of theoretical power transmission ($|S_{21}|$) and reflection ($|S_{11}|$) responses of the normalized coupling-routing diagram associated to the proposed N-passband/M-embedded-notch filtering stage in Fig. 1. (a) $N = M = 2$: $\Omega_1 = -5$, $\Omega_2 = 5$, $\Omega_{n1} = -5$, $\Omega_{n2} = 5$, and $\overline{J_{A1}} = \overline{J_{A2}} = \overline{J_{B1}} = \overline{J_{B2}} = 1$. (b) $N = M = 2$: $\Omega_1 = -5$, $\Omega_2 = 5$, $\Omega_{n1} = -5$, $\Omega_{n2} = 5$, $\overline{J_{A1}} = 1.4$, $\overline{J_{A2}} = 1$, $\overline{J_{B1}} = 1.2$, and $\overline{J_{B2}} = 0.7$. (c) $N = 2$ and $M = 3$: $\Omega_1 = -5$, $\Omega_2 = 5$, $\Omega_{n1} = -6$, $\Omega_{n2} = -4$, $\Omega_{n3} = 5$, $\overline{J_{A1}} = 1.4$, $\overline{J_{A2}} = 1$, $\overline{J_{B1}} = 1.2$, $\overline{J_{B2}} = 0.7$, and $\overline{J_{B3}} = 0.7$. (d) $N = M = 2$: $\Omega_1 = -2$, $\Omega_2 = 2$, $\Omega_{n1} = -3$, $\Omega_{n2} = 3$, $\overline{J_{A1}} = \overline{J_{A2}} = 1$, and $\overline{J_{B1}} = \overline{J_{B2}} = 1.3$.

to create TZs in their filtering transfer functions in order to achieve sharp-rejection properties into them are detailed. In all cases, supportive theoretical design examples are provided.

A. Multi-Passband/Multi-Embedded-Notch Filtering Stage

The normalized coupling-routing diagram of the proposed multi-passband/multi-embedded-notch filtering stage for a realization with N transmission bands and M in-band stopbands is shown in Fig. 1. As can be seen, following an analogous theoretical formalism as in other past works on multi-band filter synthesis although without co-designed multi-passband/multi-in-band-notch generation—e.g., [19] and [20]—, it is derived from applying the following two-term frequency transformation $\Omega \rightarrow \mathcal{F}(\Omega)$ over a normalized lowpass resonating node:

$$\Omega \rightarrow \mathcal{F}(\Omega) = \underbrace{\left(\sum_{i=1}^{N} \frac{\overline{J_{Ai}}^2}{\Omega - \Omega_i} \right)^{-1}}_{\text{Multi-passband term}} - \underbrace{\sum_{k=1}^{M} \frac{\overline{J_{Bk}}^2}{\Omega - \Omega_{nk}}}_{\text{Multi-notch term}}, \quad (1)$$

which results on a multi-resonant structure with a multi-passband and a multi-notch sub-cell—i.e., $Y_R(\Omega)$ turns out to be $Y_{MR}(\Omega)$ in Fig. 1 after applying $\Omega \rightarrow \mathcal{F}(\Omega)$ to $Y_R(\Omega)$. Here, Ω is the normalized frequency, $\Omega_1, \Omega_2, \ldots, \Omega_N$ ($\Omega_1 < \Omega_2 < \ldots < \Omega_N$) are the normalized resonant frequencies of the resonating nodes in the multi-passband sub-cell (i.e., center frequencies of the first-order passbands

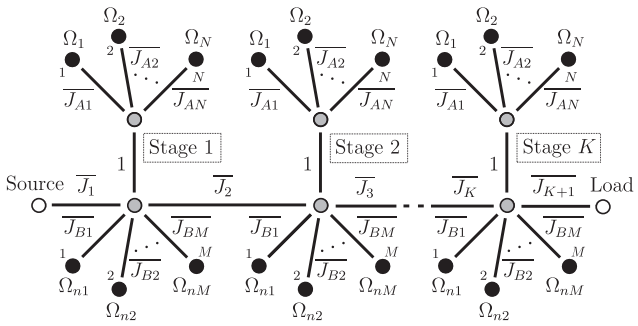


Fig. 3. Normalized coupling-routing diagram of a Kth-order filter using the in-series cascade connection of K replicas of the N-passband/M-embedded-notch filtering stage in Fig. 1.

when no in-band notches are created), $\Omega_{n1}, \Omega_{n2}, \ldots, \Omega_{nM}$ ($\Omega_{n1} < \Omega_{n2} < \ldots < \Omega_{nM}$) are the normalized resonant frequencies of the resonating nodes in the multi-embedded-notch sub-cell (i.e., center frequencies of the in-band notches), $\overline{J_{A1}}, \overline{J_{A2}}, \ldots, \overline{J_{AN}}$ are the normalized admittance-inversion constants in the multi-passband sub-cell, $\overline{J_{B1}}, \overline{J_{B2}}, \ldots, \overline{J_{BM}}$ are the normalized admittance-inversion constants in the multi-embedded-notch sub-cell, and $Y_0 = 1/Z_0$ is the reference admittance for normalization.

For illustration purposes, several examples of theoretically-synthesized power transmission and reflection responses by means of the coupling-routing diagram in Fig. 1 associated to the conceived multi-passband/multi-embedded-notch filtering stage when arranged in transmission mode—unitary normalized admittance inverters to the source and the load are used—are depicted in Fig. 2. Specifically, Fig. 2(a) and (b) show spectrally-symmetrical and asymmetrical dual-passband profiles with an embedded notch in each band, respectively. Fig. 2(c) corresponds to a dual-passband example with two embedded notches in the lower band and one notch in the upper band. Finally, Fig. 2(d) proves how two passbands and two embedded notches can be closely allocated to produce a quadruple-passband filtering profile with TZs between all passbands.

It should be noticed that, in addition to the TZs associated to the in-band notches, stopband TZs are created by the multi-passband part between each pair of contiguous transmission bands. The formulas for the normalized frequencies of these TZs for the cases $N = 2$ (i.e., dual-passband case: Ω_z) and $N = 3$ (i.e., triple-passband case: Ω_{z1} and Ω_{z2}) are as follows:

$$\underline{N = 2}: \quad \Omega_z = \frac{\overline{J_{A1}}^2 \Omega_2 + \overline{J_{A2}}^2 \Omega_1}{\overline{J_{A1}}^2 + \overline{J_{A2}}^2} \quad (2)$$

$$\underline{N = 3}: \quad \Omega_{z1}, \Omega_{z2} = \frac{b \mp \sqrt{b^2 - 4ac}}{2a}, \quad (3)$$

$$a = \overline{J_{A1}}^2 + \overline{J_{A2}}^2 + \overline{J_{A3}}^2$$

$$b = \overline{J_{A1}}^2 (\Omega_2 + \Omega_3) + \overline{J_{A2}}^2 (\Omega_1 + \Omega_3) + \overline{J_{A3}}^2 (\Omega_1 + \Omega_2)$$

$$c = \overline{J_{A1}}^2 \Omega_2 \Omega_3 + \overline{J_{A2}}^2 \Omega_1 \Omega_3 + \overline{J_{A3}}^2 \Omega_1 \Omega_2.$$

B. Higher-Order Filter Designs

By in-series cascading several replicas of the multi-passband/multi-embedded-notch filtering stage suggested in

1549-7747 (c) 2021 IEEE. Personal use is permitted, but republication/redistribution requires IEEE permission. See http://www.ieee.org/publications_standards/publications/rights/index.html for more information.
Authorized licensed use limited to: UNIVERSITY COLLEGE CORK. Downloaded on March 10,2021 at 10:54:12 UTC from IEEE Xplore. Restrictions apply.

This article has been accepted for publication in a future issue of this journal, but has not been fully edited. Content may change prior to final publication. Citation information: DOI 10.1109/TCSII.2021.3056584, IEEE Transactions on Circuits and Systems II: Express Briefs

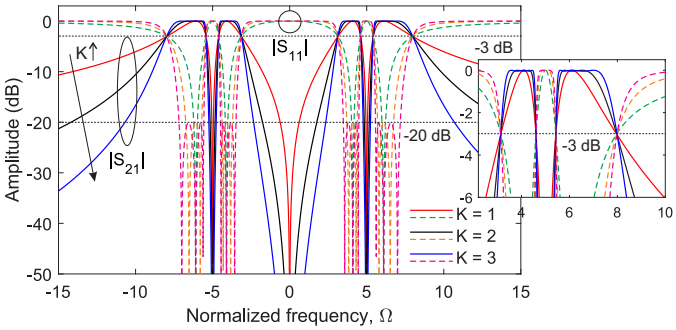


Fig. 4. Examples of theoretical power transmission ($|S_{21}|$) and reflection ($|S_{11}|$) responses of the normalized coupling-routing diagram associated to the N-passband/M-embedded-notch Kth-order filter in Fig. 3 for $K = 1, 2$, and 3 ($K = 1$: $\overline{J_1} = \overline{J_2} = 1$; $K = 2$: $\overline{J_1} = \overline{J_3} = 1.133$ and $\overline{J_2} = 1.42$; $K = 3$: $\overline{J_1} = \overline{J_4} = 1.24$ and $\overline{J_2} = \overline{J_3} = 1.35$; in all cases, $N = M = 2$, $\Omega_1 = -5$, $\Omega_2 = 5$, $\Omega_{n1} = -5$, $\Omega_{n2} = 5$, and $\overline{J_{A1}} = \overline{J_{A2}} = \overline{J_{B1}} = \overline{J_{B2}} = 1$).

Fig. 1, higher-order realizations of this filter concept can be designed. This is shown in Fig. 3, where the normalized coupling-routing diagram of a Kth-order filtering network is provided ($\overline{J_1}, \overline{J_2}, \ldots, \overline{J_{K+1}}$ are the normalized admittance-inversion constants of the admittance inverters used to cascade the stages between them and with the source and the load).

Associated to the filtering scheme given in Fig. 3 for $N = M = 2$—i.e., dual-passband case with an embedded notch inside each transmission band—, examples of theoretical power transmission and reflection responses for $K = 1, 2$, and 3 are drawn in Fig. 4. These equiripple-type examples were designed to exhibit the same 3-dB bandwidth for the passbands and the embedded stopbands, as well as minimum in-band power-matching levels of 20 dB for $K = 2$ and 3. As can be seen, higher selectivity and stopband-suppression levels are obtained as K is increased, as well as flatter passband ranges.

C. Sharp-Rejection Filters With Stopband TZs

Multi-stage filter arrangements with several out-of-band TZs based on the multi-passband/multi-embedded-notch filtering block proposed in Fig. 1 can also be realized to obtain sharp-rejection filtering characteristics into them. To this aim, two distinct TZ-generation approaches can be exploited, as detailed below:

- From the in-series-cascade multi-stage filter scheme in Fig. 3, TZs can be created by producing cross coupling between the non-resonating nodes of the multi-passband sub-cells of adjacent multi-resonant filtering sections. This is illustrated in Fig. 5(a) for a three-stage dual-band BPF example with two embedded notches within each passband (i.e., $N = 2$, $M = 4$, and $K = 3$). As proven in Fig 5(b) in which illustrative power transmission and reflection responses with minimum in-band power-matching levels of 20 dB are represented, one additional TZ below/above the lower/upper passbands and two more TZs between them are created. Note that, in this case, no frequency transformation can be applied over an initial normalized lowpass network to derive the filter scheme in Fig. 5(a), since the cross coupling is generated between those non-resonating nodes of each stage different from the ones acting as input/output nodes.
- Triples, quadruplets, or other classes of traditional cross-coupled filter schemes with stopband TZs in the normalized lowpass domain can be transformed through (1) in their multi-passband/multi-embedded-notch filter counterparts. This is exemplified in Fig. 6(a) for a triplet, where the action of the frequency transformation in (1) also converts the input/output zero-susceptance non-resonating nodes of each stage into non-zero susceptance ones (the value of the normalized susceptance is related to the normalized resonant frequency of the associated resonating node in the normalized lowpass network). A triple-passband example with an embedded notch at each passband and additional stopband TZs is provided in Fig. 6(b). As can be seen, it is derived from applying (1) over an optimization-based equiripple-type normalized lowpass design with minimum in-band power-matching level of 20 dB and one TZ at the lower stopband.

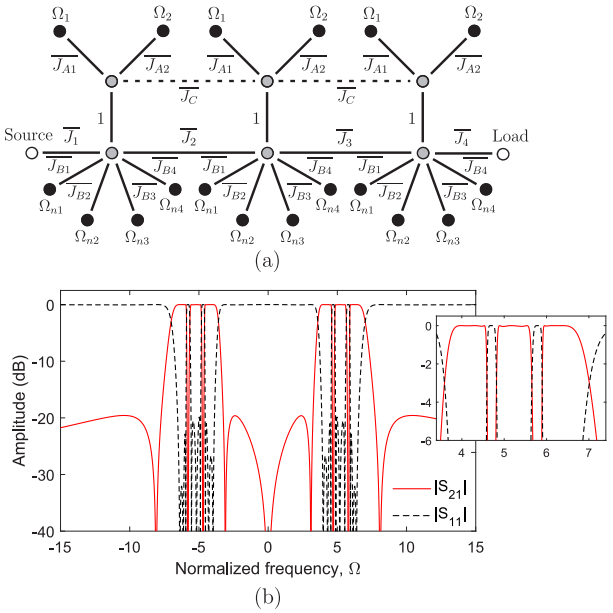


Fig. 5. Third-order filter with two passbands and two embedded notches in each transmission band and stopband TZs: cross coupling between non-resonating nodes of multi-passband sub-cells of adjacent multi-resonant filtering sections. (a) Normalized coupling-routing diagram (dashed lines: cross couplings with normalized admittance-inversion constant $\overline{J_C}$). (b) Example of theoretical power transmission ($|S_{21}|$) and reflection ($|S_{11}|$) responses ($N = 2$, $M = 4$, and $K = 3$: $\Omega_1 = -5$, $\Omega_2 = 5$, $\Omega_{n1} = -5.8$, $\Omega_{n2} = -4.7$, $\Omega_{n3} = 4.7$, $\Omega_{n4} = 5.8$, $\overline{J_{A1}} = \overline{J_{A2}} = 1$, $\overline{J_{B1}} = \overline{J_{B2}} = \overline{J_{B3}} = \overline{J_{B4}} = 0.5$, $\overline{J_1} = \overline{J_4} = 1.26$, $\overline{J_2} = \overline{J_3} = 1.4$, and $J_C = -0.1$).

III. Experimental Results

To corroborate the practical viability of the devised multi-passband/multi-embedded-notch filtering stage in higher-order filter realization, a proof-of-concept microstrip prototype of a third-order dual-band BPF with two notches embedded within the lower passband and one notch inserted within the upper transmission band has been manufactured and characterized.

To implement the resonating nodes, open-ended half-wavelength transmission-line resonators were employed, whereas the admittance inverters in the multi-passband and multi-notch sub-cells were realized by means of half-wavelength

1549-7747 (c) 2021 IEEE. Personal use is permitted, but republication/redistribution requires IEEE permission. See http://www.ieee.org/publications_standards/publications/rights/index.html for more information.
Authorized licensed use limited to: UNIVERSITY COLLEGE CORK. Downloaded on March 10,2021 at 10:54:12 UTC from IEEE Xplore. Restrictions apply.

This article has been accepted for publication in a future issue of this journal, but has not been fully edited. Content may change prior to final publication. Citation information: DOI 10.1109/TCSII.2021.3056584, IEEE Transactions on Circuits and Systems II: Express Briefs

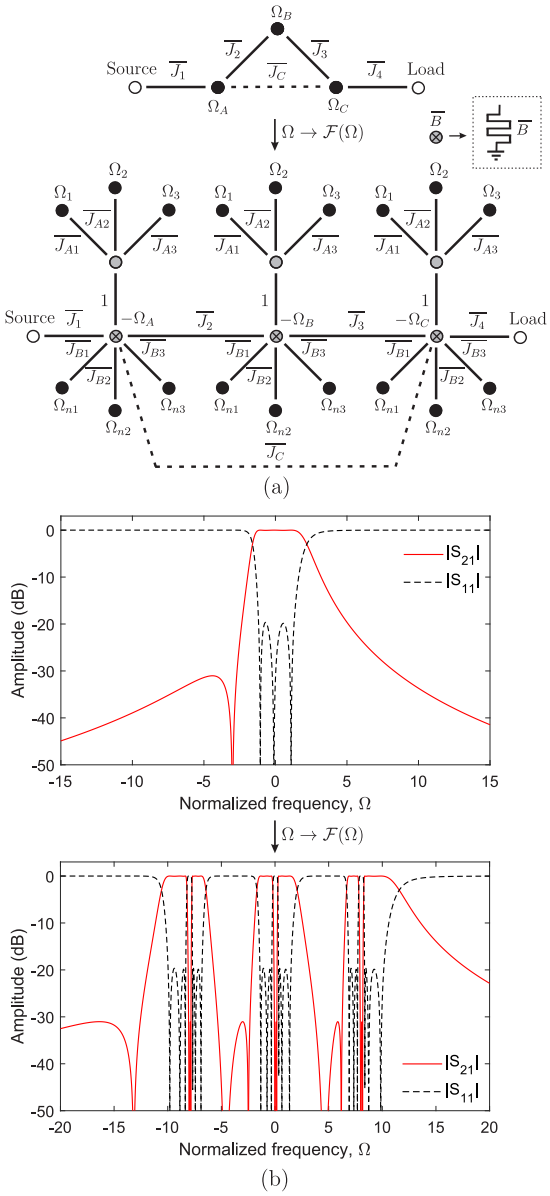


Fig. 6. Triplet in the normalized frequency domain and associated triple-passband/triple-embedded-notch filtering network after applying (1) for $N = M = 3$. (a) Normalized coupling-routing diagrams (grey circles with cross inside: non-zero-susceptance non-resonating nodes). (b) Example of theoretical power transmission ($|S_{21}|$) and reflection ($|S_{11}|$) responses ($N = M = K = 3$: $\Omega_1 = -8$, $\Omega_2 = 0$, $\Omega_3 = 8$, $\Omega_{n1} = -8$, $\Omega_{n2} = 0$, $\Omega_{n3} = 8$, $\Omega_A = \Omega_C = 0.2$, $\Omega_B = -0.47$, $J_{A1} = J_{A2} = J_{A3} = 1$, $J_{B1} = J_{B2} = J_{B3} = 0.7$, $J_1 = J_4 = 1.2$, $J_2 = J_3 = 1.18$, and $J_C = -0.55$).

transmission-line segments and lumped capacitors, respectively. For a more-compact design, one half of the resonating lines plus their adjacent transmission-line inverters in the multi-passband sub-cells were finally absorbed. Well-known filter-design techniques involving lowpass-to-bandpass-domain frequency transformation and admittance scaling were used as prior steps to pass from the corresponding normalized coupling-routing diagram (i.e., Fig. 3 for $N = 2$, $M = 3$, and $K = 3$) to this microwave-technology realization [17], [18].

The layout and a photograph of the developed microstrip prototype, along with indication of physical dimensions, are shown in Fig. 7. Its simulated (with Ansys HFSS) and

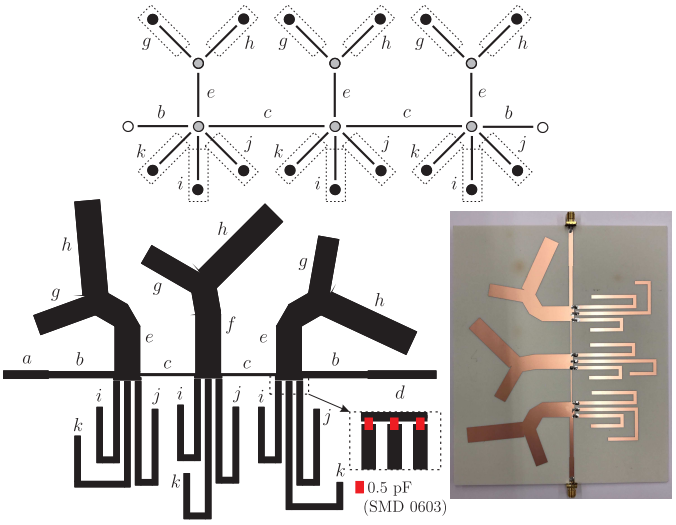


Fig. 7. Layout with associated equivalent coupling-routing diagram and photograph of the manufactured microstrip prototype (Rogers 4003C substrate: relative dielectric permittivity $\varepsilon_r = 3.38$, dielectric thickness $H = 1.524$ mm, metal thickness $t = 17.8$ μm, and dielectric loss tangent $\tan(\delta_D) = 0.0027$; lumped capacitors: 0.5 pF (± 0.25 pF as tolerance); dimensions, in mm—w stands for width and l for inner length of microstrip-line segments—: $w_a = 3.38$, $l_a = 19.7$, $w_b = 2.67$, $l_b = 29$, $w_c = 0.8$, $l_c = 24.3$, $w_d = 3.38$, $l_d = 30$, $w_e = 10.95$, $l_e = 35.6$,, $w_f = 10.95$, $l_f = 31.1$, $w_g = 9.03$, $l_g = 25.6$, $w_h = 11.03$, $l_h = 41.5$, $w_i = 2.47$, $l_i = 65.4$, $w_j = 2.47$, $l_j = 84.3$, $w_k = 2.47$, and $l_k = 88.7$).

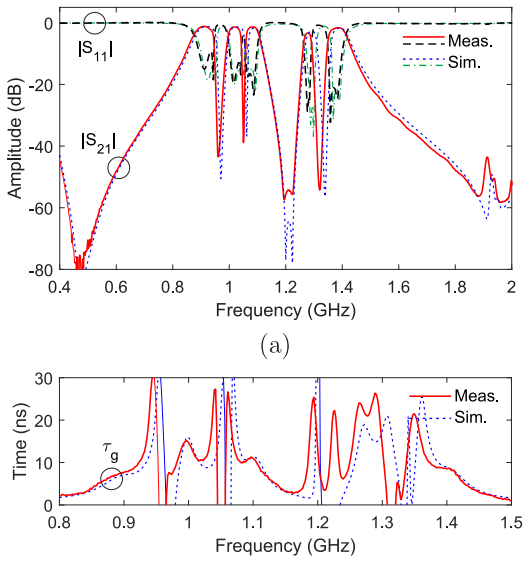


Fig. 8. Simulated and measured power transmission ($|S_{21}|$), reflection ($|S_{11}|$), and in-band group-delay (τ_g) responses of the manufactured microstrip prototype. (a) $|S_{21}|$ and $|S_{11}|$. (b) τ_g.

measured (with a Keysight 5224A network analyzer) power-transmission, reflection, and in-band group-delay responses are drawn in Fig. 8, which are in close agreement. Some minor discrepancies observed between predicted and experimental results in terms of a slight frequency shifting of the embedded in-band notches are mostly attributed to the tolerances of the lumped capacitors. The main measured characteristics of the built filter prototype for the three and two sub-transmission-bands in which the overall lower and upper passbands are split, respectively, are as follows: center

1549-7747 (c) 2021 IEEE. Personal use is permitted, but republication/redistribution requires IEEE permission. See http://www.ieee.org/publications_standards/publications/rights/index.html for more information.
Authorized licensed use limited to: UNIVERSITY COLLEGE CORK. Downloaded on March 10,2021 at 10:54:12 UTC from IEEE Xplore. Restrictions apply.

This article has been accepted for publication in a future issue of this journal, but has not been fully edited. Content may change prior to final publication. Citation information: DOI 10.1109/TCSII.2021.3056584, IEEE Transactions on Circuits and Systems II: Express Briefs

frequencies of 0.91 GHz, 1.02 GHz, 1.08 GHz, 1.28 GHz, and 1.38 GHz, 3-dB absolute bandwidths equal to 70 MHz, 45 MHz, 45 MHz, 27 MHz, and 65 MHz (i.e., equal to 7.7%, 4.4%, 4.2%, 2.1%, and 4.7% in relative terms), minimum power-insertion-loss levels of 1 dB, 1.3 dB, 1.2 dB, 3.2 dB, and 1.5 dB, and in-band power-matching levels above 9 dB, 12.8 dB, 16.4 dB, 24.8 dB, 21 dB. The measured maximum in-band group-delay variations for these sub-passbands are 23.3 ns, 17.2 ns, 16.6 ns, 6.3 ns, and 14 ns. The two lower and the upper embedded in-band notches exhibit center frequencies of 0.96 GHz, 1.05 GHz, and 1.32 GHz and rejection depths of 43.4 dB, 38.7 dB, and 54.2 dB, respectively.

Finally, Table I provides a comparison of the built dual-passband/triple-in-band-notch BPF prototype with other prior-art RF BPFs with multi-band and/or multi-notch behavior. As shown, the proposed filter configuration allows for higher number of passbands and rejection bands to be obtained.

TABLE I
COMPARISON WITH OTHER PRIOR-ART MULTI-BAND/MULTI-NOTCH BPFS

Ref.	Type of BPF	Number of sub-passbands	Number of TZs	Number of notched bands
Fig. 7 in [5]	Third-order triple-band	3	3	0
Fig. 10 in [7]	Second-order dual-band	2	5	0
Fig. 17 in [11]	Wide-band	3†	6	2
Fig. 5 in [12]	Wide-band	3†	6	2
Fig. 8 in [13]	Wide-band	3†	4	2
Fig. 13 in [14]	Wide-band	3†	6	2
Figs. 13 and 21 in [15]	Wide-band	2†	5	1
This work	Third-order dual-band	5†	7	3

†Sub-passbands attained by splitting the main passband(s) with the notch(es).

IV. CONCLUSION

An original class of co-designed multi-passband/multi-embedded-notch RF filtering stage and its coupling-routing-diagram formulation have been reported. Its theoretical usefulness in the design of higher-order RF filters with/without TZs and exhibiting various passbands and inserted in-band stopbands has been verified. Furthermore, for experimental-validation purposes, a third-order microstrip prototype of dual-passband filter with two and one embedded stopbands in the lower and upper transmission bands, respectively, has been successfully constructed and characterized. Note finally that, although here applied to an RF transmission-line-based implementation, the expounded approach for co-designed multi-passband/multi-embedded-notch filters is general for any other analog-circuit technology (e.g., lumped-element, integrated-circuit, or 3D-waveguide ones) and frequency range.

REFERENCES

[1] V. Crnojevic-Bengin, *Advances in Multi-Band Microstrip Filters*. Cambridge University Press, 2015.

[2] M. Pal and R. Ghatak, "A distinctive resonance: Multiband bandpass filter design techniques using multimode resonators," *IEEE Microw. Mag.*, vol. 16, no. 11, pp. 35–55, Dec. 2015.

[3] J.-M. Muñoz-Ferreras, R. Gómez-García, and F. Pérez-Martínez, "RF front-end concept and implementation for direct sampling of multiband signals," *IEEE Trans. Circuits Syst. II, Exp. Briefs*, vol. 58, no. 3, pp. 129–133, Mar. 2011.

[4] R. Gómez-García and A. C. Guyette, "Reconfigurable multi-band microwave filters," *IEEE Trans. Microw. Theory Techn.*, vol. 63, no. 4, pp. 1294–1307, Apr. 2015.

[5] R. Gómez-García, R. Loeches-Sánchez, D. Psychogiou, and D. Peroulis, "Multi-stub-loaded differential-mode planar multiband bandpass filters," *IEEE Trans. Circuits Syst. II, Exp. Briefs*, vol. 65, no. 3, pp. 271–275, Mar. 2018.

[6] H. Liu, Z. Wang, S. Hu, H.-X. Xu, and B. Ren, "Design of tri-band balanced filter with wideband common-mode suppression and upper stopband using square ring loaded resonator," *IEEE Trans. Circuits Syst. II, Exp. Briefs*, vol. 67, no. 10, pp. 1760–1764, Oct. 2020.

[7] J. Tang, H. Liu, and Y. Yang, "Compact wide-stopband dual-band balanced filter using an electromagnetically coupled SIR pair with controllable transmission zeros and bandwidths," *IEEE Trans. Circuits Syst. II, Exp. Briefs*, vol. 67, no. 11, pp. 2357–2361, Nov. 2020.

[8] K. Lee, T. H. Lee, C. S. Ahn, Y. S. Kim, and J. Lee, "Reconfigurable dual-stopband filters with reduced number of couplings between a transmission line and resonators," *IEEE Microw. Wireless Compon. Lett.*, vol. 25, no. 2, pp. 106–108, Feb. 2015.

[9] Y.-H. Cho and G. M. Rebeiz, "Tunable 4-pole dual-notch filters for cognitive radios and carrier aggregation systems," *IEEE Trans. Microw. Theory Techn.*, vol. 63, no. 4, pp. 1308–1314, Apr. 2015.

[10] D. Psychogiou, R. Gómez-García, and D. Peroulis, "Fully adaptive multiband bandstop filtering sections and their application to multifunctional components," *IEEE Trans. Microw. Theory Techn.*, vol. 64, no. 12, pp. 4405–4418, Dec. 2016.

[11] M. Nosrati, N. Vahabisani, and M. Daneshmand, "Compact MEMs-based ultrawide-band CPW band-pass filters with single/double tunable notch-bands," *IEEE Trans. Compon. Packag. Manuf. Technol.*, vol. 4, no. 9, pp. 1451–1460, Sep. 2014.

[12] D. Psychogiou, R. Gómez-García, and D. Peroulis, "Wide-passband filters with in-band tunable notches for agile multi-interference suppression in broad-band antenna systems," in *Proc. 2018 IEEE Radio Wireless Symp.*, Anaheim, CA, USA, Jan. 14–17, 2018, pp. 213–216.

[13] D. Psychogiou, R. Gómez-García, and D. Peroulis, "RF wide-band bandpass filter with dynamic in-band multi-interference suppression capability," *IEEE Trans. Circuits Syst. II, Exp. Briefs*, vol. 65, no. 7, pp. 898–902, Jul. 2018.

[14] R. Gómez-García, L. Yang, J.-M. Muñoz-Ferreras, and D. Psychogiou, "Single/multi-band coupled-multi-line filtering section and its application to RF diplexers, bandpass/bandstop filters, and filtering couplers," *IEEE Trans. Microw. Theory Techn.*, vol. 67, no. 10, pp. 3959–3972, Oct. 2019.

[15] X.-K. Bi, X. Zhang, S.-W. Wong, S.-H. Guo, and T. Yuan, "Design of notched-wideband bandpass filters with reconfigurable bandwidth based on terminated cross-shaped resonators," *IEEE Access*, vol. 8, pp. 37416–37427, 2020.

[16] A. Atia, A. Williams, and R. Newcomb, "Narrow-band multiple-coupled cavity synthesis," *IEEE Trans. Circuits Syst.*, vol. 21, no. 5, pp. 649–655, Sep. 1974.

[17] I. C. Hunter, *Theory and Design of Microwave Filters*. London, U.K.: IEE Press, 2001.

[18] J.-S. Hong, *Microstrip Filters for RF/Microwave Applications*, 2nd ed. New York, NY, USA: Wiley, 2011.

[19] G. Macchiarella and S. Tamiazzo, "Design techniques for dual-passband filters," *IEEE Trans. Microw. Theory Techn.*, vol. 53, no. 11, pp. 3265–3271, Nov. 2005.

[20] A. García-Lampérez and M. Salazar-Palma, "Single-band to multiband frequency transformation for multiband filters," *IEEE Trans. Microw. Theory Techn.*, vol. 59, no. 12, pp. 3048–3058, Dec. 2011.

1549-7747 (c) 2021 IEEE. Personal use is permitted, but republication/redistribution requires IEEE permission. See http://www.ieee.org/publications_standards/publications/rights/index.html for more information.
Authorized licensed use limited to: UNIVERSITY COLLEGE CORK. Downloaded on March 10,2021 at 10:54:12 UTC from IEEE Xplore. Restrictions apply.